Biochimica et Biophysica Acta 1837 (2014) 1835–1846

Contents lists available at ScienceDirect

Biochimica et Biophysica Acta

journal homepage: www.elsevier.com/locate/bbabio

Efficiency of light harvesting in a photosynthetic bacterium adapted to different levels of light

Kõu Timpmann [a], Manoop Chenchiliyan [a], Erko Jalviste [a], John A. Timney [c], C. Neil Hunter [c], Arvi Freiberg [a,b,*]

[a] Institute of Physics, University of Tartu, Riia 142, Tartu 51014, Estonia
[b] Institute of Molecular and Cell Biology, University of Tartu, Riia 23, Tartu 51010, Estonia
[c] Department of Molecular Biology and Biotechnology, University of Sheffield, Sheffield S10 2TN, UK

ARTICLE INFO

Article history:
Received 26 March 2014
Received in revised form 12 June 2014
Accepted 23 June 2014
Available online 28 June 2014

Keywords:
Photosynthesis
Photosynthetic unit
Optical spectroscopy
Light harvesting
Picosecond excitation energy transfer
Exciton

ABSTRACT

In this study, we use the photosynthetic purple bacterium *Rhodobacter sphaeroides* to find out how the acclimation of photosynthetic apparatus to growth conditions influences the rates of energy migration toward the reaction center traps and the efficiency of charge separation at the reaction centers. To answer these questions we measured the spectral and picosecond kinetic fluorescence responses as a function of excitation intensity in membranes prepared from cells grown under different illumination conditions. A kinetic model analysis yielded the microscopic rate constants that characterize the energy transfer and trapping inside the photosynthetic unit as well as the dependence of exciton trapping efficiency on the ratio of the peripheral LH2 and core LH1 antenna complexes, and on the wavelength of the excitation light. A high quantum efficiency of trapping over 80% was observed in most cases, which decreased toward shorter excitation wavelengths within the near infrared absorption band. At a fixed excitation wavelength the efficiency declines with the LH2/LH1 ratio. From the perspective of the ecological habitat of the bacteria the higher population of peripheral antenna facilitates growth under dim light even though the energy trapping is slower in low light adapted membranes. The similar values for the trapping efficiencies in all samples imply a robust photosynthetic apparatus that functions effectively at a variety of light intensities.

1. Introduction

The photosynthetic unit (PSU) of purple bacteria consists of two general types of pigment–protein complexes — the reaction center (RC) and the light-harvesting (LH, also referred to as antenna) complexes [1,2]. The main function of the LH complexes is to capture sunlight and to transfer the excitation energy to the RCs where it serves to initiate a charge separation process [3–7]. The LH complex thus plays a vital role in the energy transduction process in photosynthetic organisms, plants, algae, and bacteria, by increasing the effective cross section for solar light absorption of each RC, and by ensuring the photosynthesis function over a wide range of incident light intensity [5,8,9].

In most purple bacteria, the photosynthetic membranes contain two types of LH complexes: the core light harvesting complex 1 (LH1) and the peripheral/distal light harvesting complex 2 (LH2). While LH1 is firmly bound to RCs, LH2 transfers the excitation energy to the RCs via LH1. The major photoactive pigment in all these LH complexes is bacteriochlorophyll-a (BChl). In LH2 and LH1 complexes multiple BChl molecules are tightly packed against each other, inferring that the photoexcitation transport in bacterial membranes takes place by means of collective excitons rather than by individual excitations hopping along arrays of molecules [6,10].

To ensure that photosynthesis is effective under vastly varying environmental conditions such as light intensity and its spectral distribution, the structural composition and the related spectral properties of the PSU have to be versatile. High resolution atomic force microscopy studies of the intracytoplasmic photosynthetic membranes of bacteria have disclosed variations of the structural organization of PSU that parallel growth conditions [11–13]. In membranes from the cells grown under high light intensities (henceforth called high light (HL) adapted membranes), the number of peripheral antenna complexes available in a PSU is relatively small, whereas in low light (LL) adapted membranes, which have been harvested from the cells grown under dim light, the PSU is dominated by the peripheral antenna complexes [12,14–16]. In some other species of photosynthetic purple bacteria light adaptation involves significant modification of spectral properties as well as the structure of the distal antenna [13,16,17]. These structural and spectral adaptations allow the bacteria to accommodate different ecological niches.

It has long been observed that the fluorescence from photosynthetic bacteria, a waste when assessed from the point of view of photosynthesis efficiency, responds to the state of the photochemistry taking place

* Corresponding author at: Institute of Molecular and Cell Biology, University of Tartu, Riia 23, Tartu 51010, Estonia. Tel.: +372 56453175.
E-mail address: arvi.freiberg@ut.ee (A. Freiberg).

http://dx.doi.org/10.1016/j.bbabio.2014.06.007
0005-2728/

within the RC [18–21]. There are two well defined phases of photosynthesis in purple bacteria related to the excitation light intensity. At low excitation intensity all the RCs will be open, ready to accept excitons from the antenna; the special pair of the RC (commonly assigned to P) is reduced and available for charge separation upon photoexcitation. This phase, characterized by low antenna fluorescence yield, is named here as the "active region of photosynthesis". At high excitation intensity another phase termed the "saturated region of photosynthesis" is reached with the majority or all of the RCs in a closed state; in the closed state the special pair of the RC is oxidized (P^+) and the antenna fluorescence yield is maximal. When the excitation light intensity is kept between the active and saturated regimes, a mixed (actinic) state with some open RCs and the remaining closed RCs is created.

The fluorescence yield from the antenna can be formally evaluated as

$$\varphi_f = \frac{k_f}{k_2}, \quad (1)$$

where k_f is the fluorescence decay rate constant and $k_2 = k_f + k_t + k_{IC} + k_{ISC} + k_q$ is the total quenching rate constant via various decay routes including the fluorescence, trapping at the RC (k_t), internal conversion (k_{IC}), intersystem crossing (k_{ISC}), and quenching by still other routes (k_q). Assuming constant k_{IC}, k_{ISC}, and k_q, the variable fluorescence is due to a change of the trapping rate k_t according to the state of the RCs (see below).

The variable fluorescence is essentially related to the antenna exciton lifetime, thus providing a complementary diagnostics tool for the different photosynthesis phases by measuring the fluorescence decay time. The active regime of photosynthesis is expected to be characterized by the shortest lifetime, because of the prevailing quenching of antenna excitons by mostly reduced RCs. Under increasing excitation intensity the exciton lifetime will gradually rise, reaching a maximum at saturated regime.

When the excitation intensity is increased beyond the saturating level such that there are two or more excited states simultaneously available in the accessible radius for energy transfer, then the excited states may get annihilated and both the fluorescence yield and lifetime will drop. This excitation intensity range is further called the non-linear excitation quenching range. The first clear demonstration of this kind of behavior using picosecond time-resolved fluorescence measurements was published in [20,22] (reviewed in [1,23], see also [24]). Still, the evidence was not exhaustive, because of limited low excitation intensity range covered by these early experiments. Also, the previous work did not establish a clear, quantitative link between the fluorescence yield and the picosecond rate of fluorescence decay.

In the present work, we revisit these issues by studying membranes prepared from the *Rhodobacter sphaeroides* wild type strain 2.4.1 that has different ratios of peripheral LH2 and core RC–LH1–PufX light-harvesting complexes. As a limiting case, the set holds a mutant membrane that contains just core complexes. To the best of our knowledge, there are so far only a few and mostly theoretical studies of energy transfer in photosynthetic purple bacteria grown under different light intensities [25,26]. We use a much expanded excitation intensity range that spans the active to the saturated regimes of photosynthesis, even to the annihilation regime, with the help of different sample holding cuvettes, as detailed in Materials and methods section.

We specifically address the following fundamental question — how does the addition of peripheral antenna under low light growth influence the rate of delivery of excitation energy to the RCs and the quantum efficiency of charge separation? We also exploit the expanded excitation intensity range to explore the energy transfer time in the active and saturated states of photosynthesis, i.e., the states corresponding to mostly open and mostly closed RCs, respectively. Parallel monitoring established a direct correlation between the steady-state fluorescence yield and picosecond time-resolved fluorescence decay.

2. Materials and methods

2.1. Samples

The wild type *R. sphaeroides* strain 2.4.1 was used for the preparation of intracytoplasmic photosynthetic membrane vesicles (also called chromatophores) containing all the components of photosynthesis machinery — the LH2, LH1, and RC chromoprotein complexes. Gene expression for photosynthesis complexes in the strain 2.4.1 is dependent upon oxygen levels and light intensity, with full expression reached under anaerobic conditions under low light intensity [27,28]. The wild type chromatophore samples used in the present work (see Table 1) were prepared from cells grown anaerobically using light intensities between 100 μE/m^2/s and 1500 μE/m^2/s. The core complexes from the wild type organisms incorporate the PufX polypeptide, i.e., they (mostly) have dimeric structure [12,29–31]. PufX enables quinones/quinols to cross the LH1 barrier [32,33] and diffuse to the cytochrome bc_1 complex, a key requirement for the cyclic electron transport and for the efficient photosynthetic growth [34]. The membranes containing just LH2, LH1, or dimeric core RC–LH1–PufX complexes were prepared from a series of genetically modified mutants of *R. sphaeroides* [35]. They are indicated by adding "-only" to the name of the complex (e.g., LH2-only membrane). These mutants were grown under oxygen-limited conditions in the dark, as specified in [36].

All the membranes were prepared according to the method in [36]. Following cell disruption by French pressing the cell extracts were loaded onto 15%/40% (w/w) sucrose step gradients and centrifuged for 10 h at 27,000 rpm. Each intracytoplasmic membrane fraction was harvested from the 15%/40% interface, concentrated by centrifugation and stored in freezer at −78 °C until used. The defrosted, concentrated HL and LL samples were diluted with 20 mM TRIS (pH 7.8), the LH2-only membranes with 20 mM HEPES (pH 7.5), the LH1-only membranes with 10 mM TRIS–HCl (pH 7.9), and the RC–LH1–PufX-only membranes with 20 mM HEPES (pH 7.8) buffer solutions to obtain the optical density around 0.1 or 0.3 in the cuvette. The denser samples were usually required in fluorescence lifetime measurements to improve signal to noise ratio. The small differences in pH are unlikely to have any effect upon the pigments buried within a complex within the membrane. To mimic the fluorescence decay times in the active RC condition, the membranes were mixed with 5 mM sodium ascorbate and 25 μM phenazine methosulfate (PMS) along with the buffer solution. Reduced PMS serves as an external electron donor, supporting the cytochrome bc_1 complex in avoiding the accumulation of oxidized (P^+) states of RCs under intense illumination. The presence of ascorbate is required in order to generate reduced PMS [37]. No special precaution against environmental oxygen was taken.

Absorption spectra of the samples in buffer solution were measured using a UV/VIS spectrometer (Model V-530, JASCO Corporation) with a spectral resolution of 0.5 nm. All the measurements were performed at ambient temperature, 295 ± 3 K.

2.2. Steady state and transient picosecond fluorescence measurements

The steady state fluorescence spectrometer consists of a continuous-wave Ti: sapphire laser (3900S, Spectra Physics) pumped by a Millennia

Table 1
LH2 to LH1 ratio in the wild type chromatophore samples of *R. sphaeroides*.

Sample	LH2/LH1 absorption ratio[a]	LH2/LH1 ratio
HL116	0.89 ± 0.02	2.15 ± 0.05
HL133	1.21 ± 0.03	2.79 ± 0.07
LL181	2.02 ± 0.04	4.79 ± 0.10
LL196	2.56 ± 0.04	6.06 ± 0.10

[a] Evaluated as the ratio of integral (area) spectra of the components between 700 and 950 nm; the uncertainties here and elsewhere are the standard deviation of several independent measurements.

Prime diode pumped solid state laser (Spectra Physics) and a spectrograph (Shamrock 303i, Andor Technology) coupled with a CCD camera (DV420A-OE, Andor Technology). Two excitation wavelengths were commonly used, one at 800 nm for preferential excitation of distal LH2 complexes and another at 915 nm, for selectively exciting core RC–LH1–PufX complexes. The fluorescence was collected at 90° with respect to the direction of the excitation beam and recorded with a spectral resolution of 0.3 nm.

The picosecond time-resolved fluorescence spectrometer has been described in detail previously [38,39]. In the present configuration the set-up comprises a Coherent 700 continuous wave mode-locked dye laser with pulse duration ~3 ps synchronously pumped by an Antares 76-S Nd:YAG laser at a pulse repetition rate of 76 MHz, a double subtractive dispersion monochromator (DTMc300, Bentham Instruments Ltd.) and a home-built synchroscan streak camera system. The same setup was used for the measurements of the fluorescence lifetime dependence on the detection wavelength as well as of the fluorescence lifetime dependence on the excitation intensity. In the former case, the decay curves following excitation at 800 nm were recorded in 90° geometry between 820 nm and 960 nm using a spectral bandwidth of 4 nm. In the latter case, an excitation at 590 nm was used. This wavelength provides nearly equal excitation for all the BChl chromophores in peripheral and core complexes via their overlapping Q_x transitions. The emission from the sample was directly sent to the streak camera through a specially selected band-pass filter (F42-900 Emitter HQ 900/50, AHF Analysentechnik), which mainly transmits emission from core complexes. To cover the complete excitation intensity range required to follow the transition from active to saturated photosynthesis as well as its extension to non-linear quenching regime, the sample solution was placed either into a standard stationary quartz cuvette or into a home-built rotating cell of 5-cm diameter. The thickness of both sample holders was 2 mm. The excitation intensity was evaluated from the measured values of laser power and the laser beam spot size on the sample cell. The maximum power of the excitation laser measured with the Newport 1916-C Handheld Optical Power Meter was ~30 mW, while the spot diameter of the laser beam on the entrance surface of the cuvette was 2.0 ± 0.3 mm. The power was successively attenuated by a proper combination of neutral density filters.

2.3. Data analysis

The measured stationary spectra were corrected for spectral sensitivity of the system and processed by Origin 6.0 (OrigiLab) software.

The fluorescence decay curves were evaluated by the Spectra Solve (Version 2.0, LASTEK Pty. Ltd) software with an experimental instrument response function of ~20 ps full width at half maximum. Either a single or a double exponential approximation was applied, depending on a particular decay curve. In the latter case, the weighted average lifetime was calculated as:

$$\tau_{av} = \frac{A_1\tau_1 + A_2\tau_2}{A_1 + A_2}, \quad (2)$$

where A_1, A_2, τ_1, and τ_2 are the relative amplitude and decay time of individual decay components.

3. Results

3.1. LH2 to LH1 ratio of the chromatophores adapted to different levels of light

Fig. 1 shows the absorption spectra in the near-infrared spectral range of the two chromatophore samples designated as HL116 and LL196. These are the samples prepared under high (1500 μE/m^2/s) and low (100 μE/m^2/s) actinic irradiations, respectively. The two samples assigned as HL133 and LL181 in Table 1 show the spectra intermediate

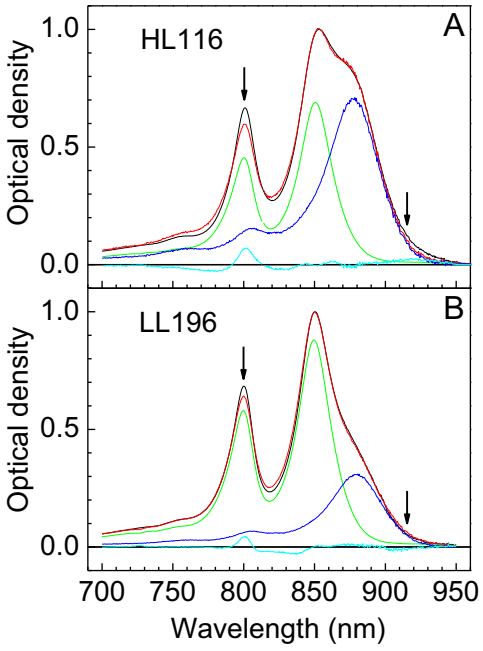

Fig. 1. Decomposition of the absorption spectra of the HL116 (A) and LL196 (B) membrane samples from wild type *R. sphaeroides* strain 2.4.1. Shown in black and red curves are the measured and simulated absorption spectra, respectively. The fitting sub-spectra of the LH2-only and RC–LH1–PufX-only membranes, correspondingly, are shown in green and blue. The difference between the measured and the simulated spectra is drawn in cyan. The arrows indicate the selective excitations used in stationary fluorescence measurements in Section 3.3.

to the ones in Fig. 1. The spectra in Fig. 1 consist of three major absorption bands peaking around 800 nm, 850 nm, and 880 nm. Identity of these spectral features is well known [40]: the 800 and 850 nm peaks (frequently called B800 and B850, respectively) arise from BChl molecules arranged into two rings at opposite sides of the LH2 transmembrane protein cylinder. The third peak at ~880 nm (B880) belongs to BChls in the LH1 complex.

The relative abundance of LH2 complexes in the LL196 membrane is clearly visible from these spectra, whereas in HL116 membranes the absorption corresponding to LH1 antenna is comparatively strong. To quantitatively evaluate the ratio of distal and core antenna complexes (LH2 to LH1 ratio or LH2/LH1 for short) the following procedure illustrated in Fig. 1 was applied, see also [41]. The absorption spectra of the chromatophore samples (shown with black line) were fitted with the sum of the absorption spectra of the mutant membranes that contained solely either the peripheral LH2 (green) or the core RC–LH1–PufX (blue) complexes (the spectra of the mutant membranes were recorded in separate experiments). For a satisfactory fit the component spectra were allowed to shift both in intensity and wavelength scale. The best fit shown in Fig. 1 with red line was achieved by shifting the absorption spectrum of the LH2-only membranes toward the red (i.e., toward longer wavelengths) by 0.5–1 nm for different samples and the spectrum of the RC–LH1–PufX-only membranes also to the red by 3.5–5.5 nm.

The difference (measured minus simulated) spectra drawn in cyan show that the fit for both samples is almost perfect (within ±2%) around the main exciton absorption bands at 825–950 nm. However, the simulated spectrum around 800 nm, where mostly B800 BChls of LH2 absorb light (the minor peak around 800 nm seen in the spectrum of RC–LH1–PufX-only membranes is contributed by RCs), is slightly lower than the measured spectrum, indicating that in the mutant LH2-only membranes the B800/B850 ratio is somewhat reduced compared to wild type samples. Still, compensating for this defect has little impact to the stoichiometry number in question.

To estimate the LH2/LH1 ratio from integral absorption spectra we have to take into account the number of absorbing BChl molecules as well as the possible variance of molecular extinction coefficients in specific protein environments. As no solid experimental evidence for the latter is available, we assume that integral absorbencies of the BChl chromophores in LH proteins are all similar. The third column of Table 1 presents the LH2/LH1 ratios evaluated on the bases of the above postulate of similar molecular integral absorbencies and the assumption that the LH2 complex includes 27 BChl molecules, whereas the RC–LH1–PufX dimer complex, 64 BChls (56 in LH1 and 4 * 2 in RC) [31,41].

As one can see from Table 1, the LH2/LH1 ratio in the membranes shown in Fig. 1 varies almost 3-fold.

3.2. Fluorescence yield and decay time dependence on the excitation intensity

The excitation light intensity dependence of the fluorescence lifetime and the relative fluorescence yield in HL116 membranes are shown in Fig. 2. The fluorescence lifetime is detected in the spectral interval of 50 nm between 875 and 925 nm where the LH1 emission mainly contributes to the signal (see Figs. 4 and 5 for the fluorescence spectra of the samples). All the lifetime traces measured until the onset of the saturated regime of excitation intensity fitted well to a single-exponential decay, although in the transition region from active to saturated regime a mixture of open and closed states of RCs exists. The lifetime traces measured beyond the saturated region of excitation intensity were fitted with double-exponential approximation, and accordingly, the average lifetime (Eq. (2)) data were plotted in Fig. 2.

The semi-logarithmic plot in Fig. 2 clearly distinguishes the three stages of photosynthesis, A–C mentioned in the Introduction from the hazardous over-illumination stage D that should be avoided in healthy organisms. At low excitation intensity, below 3×10^{-6} W/cm^2, where the entire RC pool is in its open state (active regime of photosynthesis), and effectively almost all excitons are trapped by the RCs, both the fluorescence yield and the fluorescence lifetime reach a constant and minimal value. Toward higher intensities from ~10^{-5} W/cm^2, the fluorescence yield and lifetime values increase gradually, reaching a maximum at ~6×10^{-3} W/cm^2 when all the RCs become closed (saturated regime of photosynthesis) and the fluorescence yield and lifetime achieve their maximal and uniform value. Further increases in excitation intensity beyond ~10^{-1} W/cm^2 will result in non-linear fluorescence quenching. This kind of quenching in wild type membranes of *R. sphaeroides* under high repetition rate picosecond pulse excitation was previously assigned to annihilation of singlet and triplet excitons [23,24,42–44].

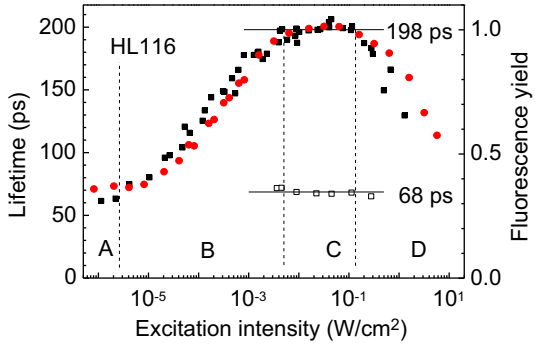

Fig. 2. Dependence of the normalized fluorescence yield (red circles) and the weighted average lifetime (black squares) on continuous wave picosecond-pulse excitation intensity in HL116 membranes. In the kinetic measurements the fluorescence was excited at 590 nm and recorded in the 875–925 nm spectral range; in the stationary fluorescence yield measurements the excitation was at 800 nm and the integration range was from 820 to 940 nm. The chemically reduced sample simulating the membranes with open RCs (open-square data) was prepared by adding 5 mM of ascorbate and 25 μM of PMS. Horizontal lines mark average fluorescence decay times in the case of mostly closed (198 ± 4 ps) and open (68 ± 2 ps) RCs. The dashed vertical lines demark qualitatively different ranges (A–D) of excitation light intensity discussed in the main text: A — active photosynthesis; B — actinic photosynthesis; C — saturated photosynthesis; D — non-linear excitation quenching.

The generally matching fluorescence lifetime and yield dependences demonstrated in Fig. 2 are typical for all the samples studied. The observed small discrepancies can be assigned to experimental uncertainties. To double check the fluorescence lifetime corresponding to active photosynthesis, the sample was mixed with ascorbate and PMS conserving the RCs in open (reduced) state. Under such condition the open-state lifetime can be safely measured using rather high intensities equivalent to saturated photosynthesis and even beyond, as demonstrated by open-square data in Fig. 2. The fluorescence decay time in the presence of exogenous electron donors is 68 ps, being in reasonable agreement with the time 62 ps measured by the low-end excitation intensity without any chemicals added.

In top part of Fig. 3A the excitation intensity dependent fluorescence lifetime and yield data are compared for the LH1-only mutant membrane sample, i.e., the core antenna membrane sample with genetically removed LH2, PufX and RCs. As in wild type membranes, the fluorescence intensity and lifetime changes are approximately parallel to each other. However, the absence of RCs qualitatively changes the character of the dependences at low excitation intensities. The yield and lifetime both keep high (in comparison with native membranes) and constant level up to the very high excitation intensity where non-linear quenching sets in. Similar behavior was detected for the LH2-only membrane sample, explicitly presented only for the fluorescence lifetime. These data convincingly prove that the change of the fluorescence response observed in wild type membranes upon increasing excitation intensity in the low intensity range is related to the availability of RCs. It is also interesting to notice that in mutant antenna-only

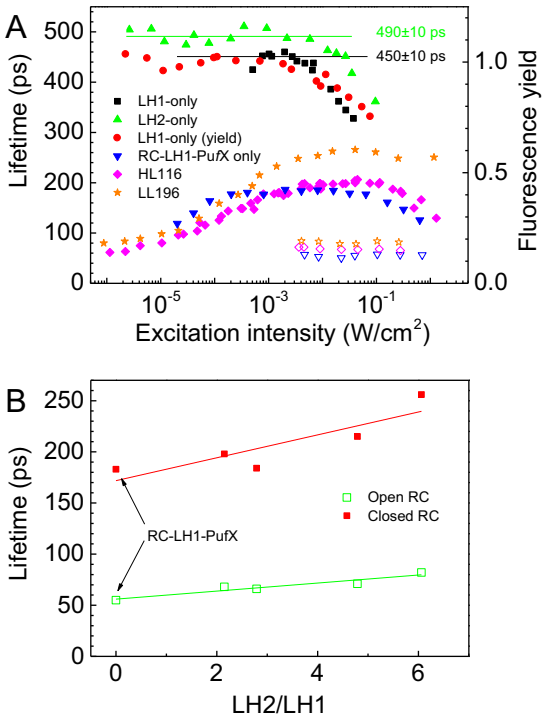

Fig. 3. (A) Dependence of the averaged lifetime of the spectrally integrated fluorescence on excitation intensity for the LH1-only (black squares) and LH2-only (green triangles) membranes, for the LL196 (orange stars) and HL116 (pink diamonds) wild type membranes, and for the mutant RC–LH1–PufX-only membrane (blue triangles). Open data points correspond to the lifetimes of respective chemically reduced samples. Shown in red dots is the normalized fluorescence yield for the LH1-only membranes. (B) The dependence of the integrated fluorescence lifetime corresponds to active (green) and saturated (red) ranges of photosynthesis on the LH2 to LH1 protein ratio. Lines represent linear fits of the data. In all cases the fluorescence was excited at 590 nm. Arrows indicate the points corresponding to the RC–LH1–PufX-only membrane.

membranes the threshold for the non-linear quenching is ~1.5 orders of magnitude lower than it is in wild type samples. This observation most probably reflects important variances in the structure and size of wild type and mutant membranes. For example, electron microscopy and atomic force microscopy of membranes from LH2-minus mutant revealed flattened membrane sheets and extended hexagonally packed RC–LH1 complexes [29,45]. LH2-only membranes on the other hand form spherical vesicular structures 50–60 nm in diameter [46]. Finally, membranes from a mutant that assembles only dimeric RC–LH1–PufX complexes tend to form tubular structures [29,30].

The lower part of Fig. 3A shows dependences of the spectrally integrated fluorescence lifetime on excitation light intensity for the two wild type membrane samples with the smallest (HL116) and the greatest (LL196) LH2 to LH1 ratio. The compared traces are fairly parallel to each other, the lifetimes of LL196 being at all times greater than those of HL116. The dependences for the rest two wild type samples with intermediate LH2/LH1 values conveniently dwell between these limiting cases. As seen in the figure, qualitatively very similar dependency was as well achieved for the RC–LH1–PufX-only membrane.

Fig. 3B implies that average lifetimes corresponding to low (open RCs) and high (closed RCs) excitation intensity limits in wild type and mutant membrane samples increase in linear fashion with the LH2 to LH1 ratio. From Table 2 it appears that despite the systematic increase of the lifetimes corresponding to closed and open states, their ratio is within the experimental uncertainty constant and close to 3. A similar change of the fluorescence yield upon closing RCs was obtained for the M21 mutant membrane of *R. sphaeroides* [21].

These observations can be rationalized as follows. The peripheral antenna network found in LL adapted membranes is more extended in comparison with HL adapted membranes. Under low excitation light intensity almost all RCs are active, the explored membrane region before trapping is minimal, and correspondingly, average exciton lifetime is short. At high excitation intensity most of the RCs are closed, allowing larger portions of the membrane to be explored before trapping which increases the average lifetime of excitons. The RC–LH1–PufX-only membrane has no distal antenna [29,30] resulting in the shortest possible fluorescence lifetimes. The fact that the saturated state lifetime in RC–LH1–PufX-only membranes appears significantly shorter than in LH1-only membranes speaks for quenching of excitons by closed RCs, as explained in [29,30].

3.3. Steady-state fluorescence spectroscopy upon preferential excitation into the LH2 and LH1 antenna compartments

The previous section established the dependence of integral fluorescence lifetime and yield on excitation intensity in HL and LL adapted samples. The present section investigates the shapes of the stationary fluorescence spectra of these samples upon excitation at selected wavelengths and the change of the spectra with excitation intensity, in response to the change of the RC state. The two different excitation wavelengths considered here excite predominantly either LH2 (at 800 nm) or LH1 (at 915 nm) antenna compartments. These preferential excitations are indicated by arrows in Fig. 1; this figure also points out the amounts of absorption by LH1 and LH2 in the corresponding regions, allowing the evaluation of the excitation branching between the compartments of the samples.

Table 2
Integrated fluorescence lifetimes corresponding to active and saturated ranges of photosynthesis.[a]

Sample (LH2/LH1)	τ_{av} (ps)		τ_{av}(closed)/τ_{av}(open)
	Active	Saturated	
RC–LH1–PufX (0)	55 ± 2	183 ± 5	3.3 ± 0.4
HL116 (2.15)	68 ± 2	198 ± 4	2.9 ± 0.4
HL133 (2.79)	66 ± 2	184 ± 7	2.8 ± 0.4
LL181 (4.79)	71 ± 2	215 ± 5	3.0 ± 0.4
LL196 (6.06)	82 ± 3	256 ± 7	3.1 ± 0.4

[a] The fluorescence signal in these measurements was integrated between 875 and 925 nm.

The fluorescence spectra shown in Fig. 4 at both excitation wavelengths reveal two distinct bands, one peaking at about 860 nm and the second at about 895 nm. These bands are related to the B850 and B880 absorption bands of the LH2 and LH1 complexes, respectively (see, e.g., [47]). It is immediately obvious from comparison of Fig. 4A and B that the higher population of peripheral antennae in the LL grown membrane in comparison with that in the HL grown membrane results in stronger fluorescence emission from the LH2 region in the LL grown membrane. It can also be seen that relative intensity of the B850 emission band depends on the excitation wavelength, being distinctly more prominent at 800-nm excitation compared with 915-nm excitation. In the latter case the spectrum does not change on excitation intensity within the actinic range of intensities.

Earlier studies [48,49] have established that direct excitation into the B880 absorption band results in thermal equilibrium distribution of excitons between the LH1 and LH2 complexes of *R. sphaeroides*. At 915-nm excitation the excitons in LH2 complexes do not get directly excited (see Fig. 1), but the corresponding energetically "up-hill" states can be populated by thermally induced energy transfer processes in membranes with closely packed LH1 and LH2 proteins [49]. The notable enhancement of the B850 fluorescence under 800-nm excitation is rather expected in case of finite transfer rate of excitons between the LH2 and LH1 compartments. The B850 fluorescence increases relative to the B880 fluorescence; the slower the transfer, the greater the LH2/LH1 ratio.

Significant change of the fluorescence spectrum with excitation intensity at 800 nm is also observed in Fig. 4. At low intensity ($\sim 10^{-5}$ W/cm^2) corresponding to active photosynthesis the weak and noisy spectrum drawn by black curve reveals prominent LH2 contribution. As can be seen from red spectrum, the LH2 part becomes relatively much smaller at saturating intensities ($\geq 3 \times 10^{-3}$ W/cm^2), being still more prominent than it is under the equilibrium 915-nm excitation (blue spectrum). The distinction of the LH2 contribution at low intensity can be most obviously explained by comparable rates of the energy

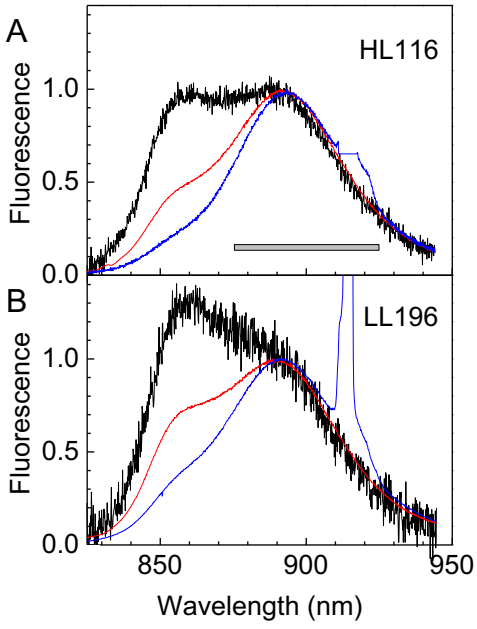

Fig. 4. Normalized fluorescence spectra of the HL116 (A) and LL196 (B) samples excited at 800 nm (black and red curves corresponding to active and saturated ranges of photosynthesis, respectively) and at 915 nm (blue curves). All the spectra are normalized at 890 nm. The feature at 915 nm is a scattered excitation light artifact. The gray bar indicates the integration range applied at kinetic measurements.

transfer from peripheral antenna to core antenna and the quenching of the LH1 excitons by open RCs. At high intensity most of the RCs are closed and the quenching rate slows down. As a consequence, population of excitons in the LH2 and LH1 compartments approaches an equilibrium value, not quite equaling it.

As follows, we will illustrate these qualitative conclusions by de-convoluting the fluorescence spectra of the LL196 sample measured at different excitation wavelengths and intensities, see Fig. 5A to C. A procedure similar to that used for the absorption spectra in Fig. 1 was applied, except that separately measured fluorescence spectra of the LH2-only and RC–LH1–PufX-only membranes were used as the fitting components and that spectral decomposition was performed using energy rather than wavelength scale.

At 800-nm excitation, the branching of absorbed photons between the LH2 and LH1 compartments takes place due to overlap of their absorption spectra, see Fig. 1. As shown in Table 3, in the particular case of the LL196 sample the branching ratio was estimated to be ~95:5 in favor of LH2 excitations. This number was achieved by assuming, in analogy with the results of [50–53], that ~20% of the excitations absorbed by RC at 800 nm escape trapping and return to LH1. In fact, the de-trapping effect on the LH2/LH1 branching ratio is minor, <2%, and can largely be discarded.

Panels A and B of Fig. 5 demonstrate the de-convolution of the fluorescence spectra for the LL196 sample upon 800-nm excitation that corresponds to active (A) and saturated (B) regimes of photosynthesis; panel C shows the decomposition under 915-nm excitation. A single excitation light intensity is used in the latter case, since the spectrum did not change over the whole actinic excitation intensity range.

There is a significant decrease of F850 (i.e., the fluorescence of LH2 related to B850) relative to F880 (the fluorescence related to B880) with increasing excitation intensity at 800 nm. At 915-nm excitation (Fig. 5C) that creates a thermal equilibrium population of antenna excitons in the LH2 and LH1 pools, the contribution of F850 is always much smaller compared with that of F880 (see Table 3). This contribution is expected to follow the LH2/LH1 ratio, which it indeed does, as shown by the data in Fig. 5D. Please notice that linear fit of the data of wild type samples nicely extrapolates to zero, which corresponds to the RC–LH1–PufX-only mutant sample.

3.4. Spectrally resolved picosecond exciton equilibration

Compared with the HL adapted chromatophores the share of F850 is always greater in LL samples, regardless of the RC state, see Table 3. Given the similar energy gap between the B850 and B880 absorption bands in these samples, this higher level of F850 could only be caused by a longer average energy transfer time between the LH2 and LH1 complexes in LL chromatophores due to a more extended LH2 system [12,13]. Therefore, in the following, we studied the change of the fluorescence lifetime with the emission wavelength.

Fig. 6 shows the wavelength dependence of the fluorescence lifetime for the LL196 and HL116 chromatophore samples excited at 800 nm. In this case, excitons in the LH2 antenna are primarily generated, providing the largest contrast between exciton equilibration and trapping times. The used excitation intensity slightly exceeded the actinic range, but was necessary for obtaining reasonable signal to noise ratio at short wavelengths where the dispersed fluorescence signal becomes very weak.

The fast dynamics of tens of picosecond duration that describes exciton transfer and equilibration between the LH2 and LH1 antenna compartments is most clearly seen around 820–880 nm, in the fluorescence range of the B850 excitons of LH2. Above 880 nm, an order of magnitude longer decay time is observed that does not change with the wavelength. This single-exponential decay is mostly governed by quenching of the B880 excitons of LH1 with closed RCs [54,55]. The experimental decay times corresponding to blue (820–850 nm) and red (910–960 nm) parts of the fluorescence spectrum are listed for all samples in Table 4. These present observations are in qualitative agreement with the earlier data [20,24,56,57].

The lifetimes τ_{av} in Table 2 under saturated excitation condition (when F880 dominates over F850, see Fig. 5B) should be, and actually are, comparable with the corresponding long-wavelength data in Table 4, except that the decay times reported in Table 4 are by 8–13%

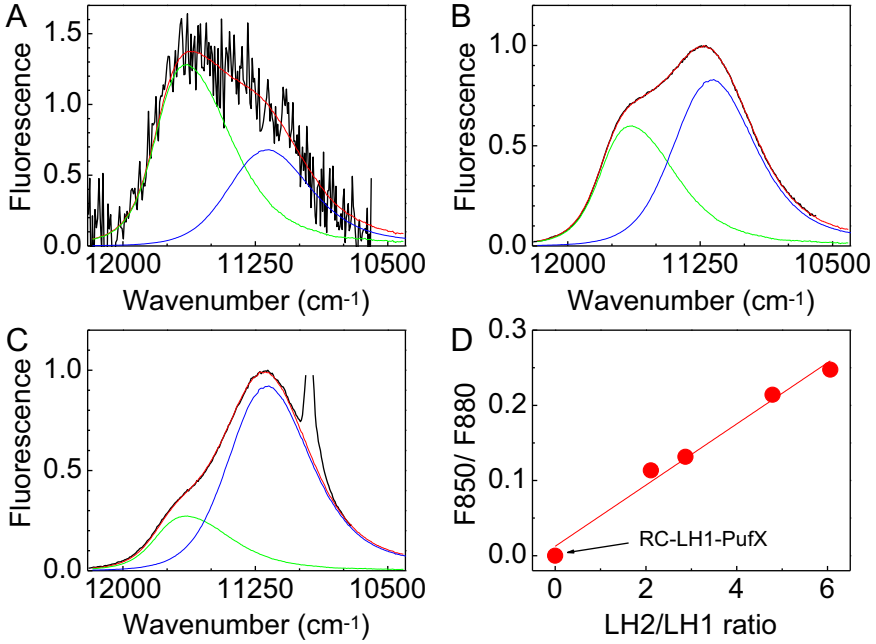

Fig. 5. (A–C) De-convolution of the LL196 fluorescence band into sub-bands corresponding to emission of the LH2 and LH1 antenna components at 800-nm excitation (A and B) and at 915-nm excitation (C). All spectra are normalized at 890 nm. The spectra in panel A represent active state of photosynthesis (excitation intensity of 3.6×10^{-6} W/cm^2), while the spectra in B and C represent saturated state of photosynthesis (excitation intensities of 3.5×10^{-2} W/cm^2 and 4.6×10^{-3} W/cm^2, respectively). The experimental spectra are drawn in black, the fitted spectra in red, and the fit component spectra in green (LH2) and blue (RC–LH1–PufX). (D) Dependence of the relative fluorescence yield, F850/F880, on the LH2 to LH1 ratio at 915-nm excitation. The line connecting the data points represents a linear fit of the data. Arrow indicates the point corresponding to the RC–LH1–PufX-only membrane.

Table 3
Ratio of fluorescence intensities corresponding to the LH2 and LH1 sub-bands at active and saturated limits of photosynthesis upon 800-nm and 915-nm excitation.

Excitation wavelength (nm)	Sample[a]	Excitation intensity (W/cm^2)		F850/F880	
		Active ($\times 10^{-6}$)	Saturated ($\times 10^{-2}$)	Active	Saturated
800	HL116 (86:14)	4.0	6.4	0.86 ± 0.02	0.32 ± 0.01
	HL133 (87:13)	2.8	6.4	0.85 ± 0.02	0.38 ± 0.01
	LL181 (93:7)	3.3	1.7	0.95 ± 0.03	0.45 ± 0.01
	LL196 (95:5)	3.6	3.5	1.56 ± 0.05	0.60 ± 0.01
915[b]	HL116 (0:100)	3.2×10^{-2}		0.114 ± 0.002	
	HL133 (0:100)			0.132 ± 0.002	
	LL181 (0:100)			0.214 ± 0.004	
	LL196 (0:100)			0.248 ± 0.006	

[a] Shown in parentheses is the LH2/LH1 excitation branching ratio at 800-nm excitation.
[b] Data do not depend on excitation intensity.

shorter. This discrepancy is due to the slightly too high excitation intensity used in dispersive fluorescence measurements, as clarified above. The short-wavelength decay time around 20–30 ps shows a weak correlation with LH2/LH1, arising abruptly to ~45 ps in the case of the LL196 sample with most extensive LH2 antenna pool.

In the light of the data in Table 4, it is evident that in the HL samples with small LH2 antenna pool, the fluorescence decay times all over the spectrum are shorter than in the LL samples, where the number of LH2 complexes is larger. Qualitatively similar results have been obtained on green bacteria [58] as well as of individual photosystems of green plants [59,60] and cyanobacteria with different antenna sizes [61]. However, acclimation of the photosynthetic apparatus to the environmental conditions in full plants and cyanobacteria is a vastly complex phenomenon, still not understood in detail (see Refs. [62,63] for a review). This once again implies that the HL adapted species are more efficient in delivery of excitation energy into the energy trapping/quenching core complex than the LL adapted species, and that the only, albeit vital, justification for the large peripheral antenna in LL samples is the survival under poor illumination conditions.

4. Discussion

In Section 3.2, we found that trapping of excitons by the RC takes always longer in LL samples than in HL samples, regardless of the state of RC. This finding was tentatively explained by the more extended peripheral antenna network in the LL adapted membranes. The shapes of the stationary fluorescence spectra described in Section 3.3 corroborate this interpretation by contributing a higher LH2 fluorescence signal in the LL membranes compared with the HL samples, irrespective of the excitation wavelength. Direct excitation into the LH1 antenna at 915 nm causes only a weak LH2 fluorescence, as it originates from the energetically unfavorable back transfer from the LH1 antenna pool. Due to equilibrium nature, its relative contribution is independent of the RC state, and thus the excitation intensity. This is in contrast to preferential excitation into the LH2 pool, when the contribution of the LH2 fluorescence strongly depends on excitation intensity driving the RC state. The spectrally resolved lifetime measurements described in Section 3.4 revealed a slowdown of energy transfer from LH2 to LH1, in accordance with the LH2 to LH1 ratio.

The greater share of the LH2 fluorescence in LL samples throughout the entire actinic range of photosynthesis raises the possibility that energy transfer within the peripheral antenna compartment and between the LH2 and LH1 compartments might be slower than commonly assumed. To validate this suggestion, the experimental stationary and time resolved fluorescence results were analyzed adopting a kinetic model described in Appendix A.

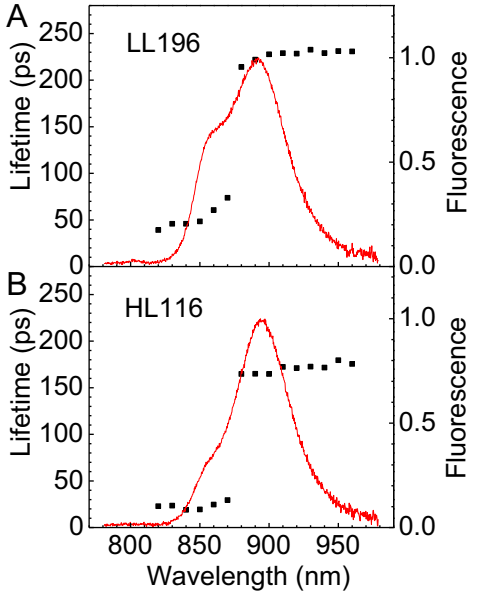

Fig. 6. Dependence of the averaged fluorescence lifetime as a function of the emission wavelength for the LL196 (A) and HL116 (B) membranes. Fluorescence was excited at 800 nm using excitation intensity of 0.25 W/cm^2. The normalized stationary fluorescence spectra of the samples excited at 590 nm are also presented for reference.

4.1. Model evaluations of rate constants as a function of the LH2 to LH1 ratio

Our aim is to find the microscopic rate constants compatible with the experimental ratios of fluorescence yield from the LH1 and LH2 antennas and with the fluorescence decay times measured with varying excitation wavelength and intensity. Analysis of the experimental decay curves brings out two apparent rate constants, which in Appendix A are denoted by γ_1 and γ_2. They incorporate all the microscopic rate constants k_1, k_{-1}, k_2, and k_{loss} of the applied model, see Eq. (A3). The decay time of excitons in the LH2-only membrane, $1/k_{\mathrm{loss}}$, has literature values around 700 ps [50,64], while the present measurements demonstrated in Fig. 3A returned 490 ± 10 ps. Since the influence of k_{loss} on the results is small (as long as $k_{\mathrm{loss}} \ll k_1$), this latter value was used in current calculations. By knowing γ_1, γ_2, and k_{loss}, the remaining rate constants (k_1, k_{-1}, and k_2) can be evaluated with the help of Eqs. (A3) and (A4). The ratio of the fluorescence yields in the case of selective excitation into either the LH2 or LH1 antenna was calculated according to Eq. (A6).

Table 4
Decay times at short-wavelength (≤850 nm) and long-wavelength (≥910 nm) edges of the fluorescence spectrum at saturated excitation intensity.

Sample (LH2/LH1)	τ_{av} (ps)	
	≤850 nm	≥910 nm
HL116 (2.15)	21.2 ± 2.3	174 ± 5
HL133 (2.79)	23.2 ± 3.5	169 ± 4
LL181 (4.79)	27.4 ± 4.9	188 ± 9
LL196 (6.06)	44.8 ± 3.9	230 ± 5

In reasonable approximation the τ_{av}^{-1} values in Table 2, measured over the LH1 fluorescence range under the condition of active and saturated photosynthesis, correspond to γ_2 with open (γ_2^o) and closed (γ_2^c) RCs, respectively. γ_1 evaluated from the data of Table 4 at ≤850 nm is experimentally available only in case of closed RCs (γ_1^c). However, since according to our model, k_1 and k_{-1} are not supposed to depend on the state of RC, k_2 as well as γ_1 under active photosynthesis condition with open RCs (i.e., γ_1^o) can both be evaluated from the existing data.

The calculated inverse rate constants or corresponding transfer times for the four wild type samples are listed in Table 5. In Fig. 7 these data are plotted as a function of the LH2/LH1 ratio together with experimental decay times.

It is seen from Table 5 and Fig. 7 that the forward energy transfer time, k_1^{-1}, between the LH2 and LH1 antennas grows regularly and significantly with LH2/LH1, being ca. 2.5 times bigger in the LL196 sample than in HL116. At the same time, the backward energy transfer time k_{-1}^{-1} behaves rather unevenly, first decreasing and then increasing with LH2/LH1. In case of k_2, which is responsible for trapping (open RC, k_2^o) or quenching (closed RC, k_2^c) of excitations, a very weak if any dependence on LH2/LH1 is expected, because the trapping/quenching processes occurring in the core compartment are considered similar in all four samples. This expectation is held rather well, since the k_2^{-1} values measured in different samples deviate from their mean value (53.5 ps and 191 ps in case of active and saturated photosynthesis, respectively) by not more than 10–15%.

It is obvious from Fig. 7 that the fluorescence lifetime of LH1 identified with $(\gamma_2^c)^{-1}$ is under saturated conditions significantly controlled by k_2^c. No such relationship between $(\gamma_2^o)^{-1}$ and k_2^o is observed. Another interesting feature to note in Fig. 7 is that when the longer decay times, γ_2^{-1}, strongly vary with closing RC in response to increasing excitation intensity, the shorter times, γ_1^{-1}, change only slightly; consequently, they are also not affected by k_2.

Consistency of the microscopic rate constants obtained from the analysis of fluorescence kinetics can be further evaluated by comparison with the measured and calculated (according to Eq. (A6)) steady state fluorescence yield data. The required for the calculations rate constants and equilibrium constants were taken from Table 5, while the branching ratios upon excitation into the LH2 and LH1 compartments are available in Table 3. The results of such evaluations in the case of the HL116 and LL196 samples are shown in Fig. 8; data for the remaining two wild type samples are qualitatively similar.

In Fig. 8, the calculated curves at 915-nm excitation follow Eq. (3):

$$F_{850}/F_{880} = (K(1 + k_{loss}/k_1))^{-1} \quad (3)$$

that results from Eq. (A6) at $j = 0$. According to Eq. (3), the ratio F_{850}/F_{880}, which has an initial value of $1/K$, decreases with increasing k_1^{-1}, because at constant K the slowing down of the forward transfer rate also reduces the back transfer rate (see Eq. (A4)).

Direct population of LH2, as in the case of 800-nm excitation, leads to an increase of F_{850}/F_{880} (compared to 915-nm excitation), which also depends on the RC state. An approximation of Eq. (A6) relevant for this case is obtained by neglecting the small $k_{loss}(1 - j)$ term in the denominator:

$$F_{850}/F_{880} = 1/K + jk_2k_1^{-1}. \quad (4)$$

Eq. (4) is a linear function of k_1^{-1} with a positive slope equal to jk_2. The slope is steeper at larger k_2 values corresponding to open RC.

In an ideal case, the calculated and experimental fluorescence yield ratios for each sample would equal each other at one and the same k_1^{-1} value. One thus expects that the three calculated inclined lines in Fig. 8 cross the respective horizontal dotted lines at similar k_1^{-1} values. Furthermore, such determined inverse rates should overlap with

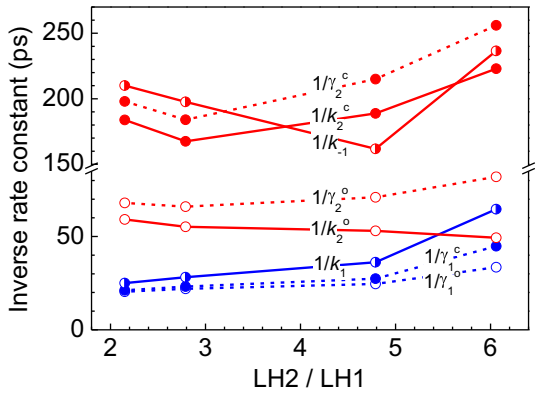

Fig. 7. Dependence of the inverse apparent (dotted line) and microscopic (solid line) rate constants on the LH2 to LH1 protein ratio. Open and closed symbols of the data points indicate the state of RC. The half-open symbols represent lifetimes that are the same for both RC states. Data regarding LH2 and LH1 compartments are indicated by blue and red colors, respectively.

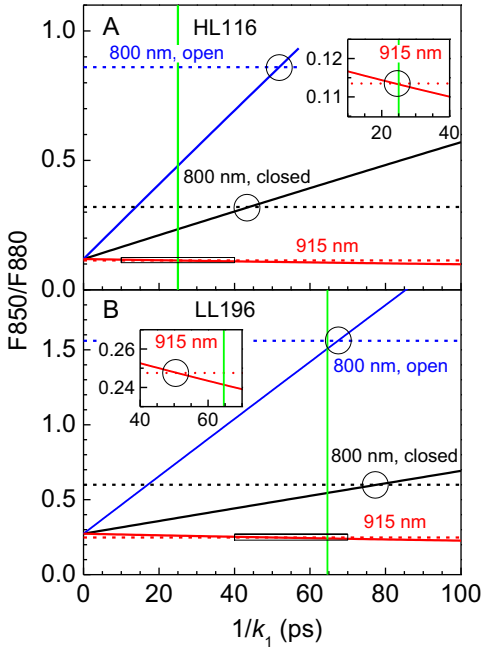

Fig. 8. Dependence of the calculated relative fluorescence yield (shown with inclined black, blue, and red solid lines) on the forward energy transfer time, k_1^{-1}, for the HL116 (A) and LL196 (B) samples. The measured values of F_{850}/F_{880} are represented by dotted horizontal lines. Black and blue colored lines correspond to the 800-nm excitation in the case of closed and open RCs, respectively, while red lines to the 915-nm excitation, for which the yield ratio is independent on the RC state. Green vertical lines denote the k_1^{-1} values obtained from kinetic data. The rings indicate intersections between the experimental and calculated values of F_{850}/F_{880}. Insets are blow-ups of the areas delineated by rectangles. See text for further details.

Table 5
The calculated forward energy transfer time, k_1^{-1}, backward energy transfer time, k_{-1}^{-1}, equilibrium constant, K, and quenching time by RCs, k_2^{-1}.

Sample (LH2/LH1)	k_1^{-1} (ps)	k_{-1}^{-1} (ps)	$K = k_1 / k_{-1}$	k_2^{-1} (ps)	
				Active	Saturated
HL116 (2.15)	25	210	8.40	59	185
HL133 (2.79)	28	200	7.01	55	170
LL181 (4.79)	36	160	4.47	52	190
LL196 (6.06)	65	235	3.66	48	220

the values of k_1^{-1} determined from time-resolved measurements (see Table 5).

As can be seen in Fig. 8, this stringent condition is nowhere nearly met. Only in HL116 sample at 915-nm excitation a triple-crossing of the red horizontal, green vertical, and red negatively sloped curves is observed, but the interceptions (shown by circles) of the calculated and experimental relative yields at 800-nm excitation that correspond to open and closed RCs do not quite occur at the same k_1^{-1} value. Notably also, the crossings systematically take place at larger arguments than the k_1^{-1} determined from kinetic measurements (indicated by vertical green line).

Experimental and modeling uncertainties aside, the above systematic discrepancy can be explained by the presence of a small number of disconnected LH2 units that transfer their excitation to LH1 very slowly or not at all. Since the fluorescence from regular LH2 units is strongly quenched by fast energy transfer to LH1, even a small amount of unconnected LH2 can significantly contribute to F_{850}, and thereby, to an increase of F_{850}/F_{880}. One can estimate the share of disconnected LH2 in the whole LH2 antenna pool by bringing down the observed fluorescence yield ratio until the k_1^{-1} values evaluated for the three experimental cases match each other. Even in the worst case, this share was found <5%, but somewhat surprisingly, it always appears larger in HL samples than in LL samples. This latter fact may point to the presence of some biosynthetic precursor membranes, called UPB [65], in the HL sample. Such membranes, which are derived from sites of membrane development close to the cell wall [66], are known to comprise up to a third of all the intracytoplasmic membrane in HL cells [12]. Furthermore it was shown many years ago [67] and corroborated more recently [12] that UPB is intrinsically less efficient than intracytoplasmic membranes in terms of LH2 to LH1 energy transfer.

4.2. Quantum efficiency of primary processes of photosynthesis in R. sphaeroides

In the following we estimate, based on the obtained microscopic rate constants, the effect of the LH2/LH1 ratio on the quantum efficiency of primary stages of photosynthesis. In first approximation, since the transfer of excitons from LH2 to LH1 in wild type membranes is almost 20 times faster than the fluorescence decay time in the LH2-only membrane, one can assume a complete transfer of LH2 excitons to the core antenna, so that the only efficiency that counts is the efficiency of the LH1 antenna. The quantum efficiency can be calculated as the ratio of the trapping rate of the LH1 excitons by open RCs and the rate of creating excitons in the LH2 and LH1 pools by the incoming light, see Appendix A and References [50–53,68]:

$$\eta = \frac{k_t^0}{k_2^0}, \tag{5}$$

where k_t^0 is the trapping rate constant and $k_2^0 = k_f + k_{IC} + k_{ISC} + k_q + k_t^0$ is the total quenching rate constant under conditions of open RCs. In a good approximation, $(k_f + k_{IC} + k_{ISC} + k_q)^{-1}$ can be equated to the measured fluorescence decay time of the LH1-only membrane sample; as determined from the data of Fig. 3A, this value is 450 ± 10 ps. The trapping rate k_t^0 for each sample can then be calculated by subtracting $k_f + k_{IC} + k_{ISC} + k_q$ from the averaged overall samples' value of k_2^0 given in Table 5. The calculations yield $(k_t^0)^{-1} = 60.7$ ps for the trapping time and $\eta = 88.1\%$ for the efficiency. Under the assumption of negligible loss from LH2 neither of these quantities depends on LH2/LH1. The same numbers also characterize the mutant membrane lacking LH2 complexes. The maximum efficiency of $\eta = 88.1\%$ corresponding to lossless exciton transfer is indicated by an arrow in Fig. 9.

Real antennas have losses. In Appendix A, also a more general equation is derived that along with the well-connected LH2 antenna pool allows contribution of ill-connected or disconnected LH2 with inhibited transfer of excitons to LH1. The calculated quantum efficiencies by Eq. (A10) are shown in Fig. 9. One can see that at 915-nm excitation the drop of efficiency with increasing peripheral antenna size is minor (1–2%), because only a small proportion of LH2 complexes is populated by up-hill energy transfer from the LH1 pool. The efficiency is significantly reduced when 800-nm light is used to preferentially excite the LH2 pool. This reduction perfectly follows the slow-down of the LH2 to LH1 transfer rate, k_1. Malfunctioning antennas further decreases the efficiency, as shown in Fig. 9 for the case of 2% detached LH2 complexes.

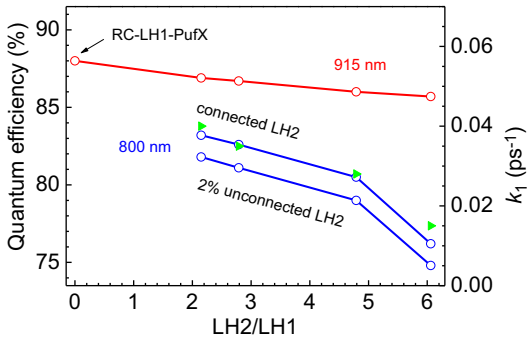

Fig. 9. Dependence of quantum efficiency of active photosynthesis on the LH2 to LH1 protein ratio upon excitation at 800 nm (blue symbols) and at 915 nm (red symbols). Arrow and RC–LH1–PufX designate the efficiency of sole core complexes. Green triangles and right scale relate to the forward energy transfer rate, k_1. The lines connecting data points are for guiding the eye.

5. Summary

We have studied the excitation intensity dependent spectral and kinetic fluorescence response of the chromatophore membranes from *R. sphaeroides*, grown under high and low light conditions. The much-expanded (over 8 orders of magnitude) coverage of excitation intensity allowed us to follow the photosynthesis from active to saturated state. As the LL adapted membrane has more peripheral LH2 complexes, the trapping of the absorbed energy by the RC is delayed owing to an elongated energy transfer path; in the HL adapted membrane sample with less number of peripheral antennas, the trapping was found to be much faster. By incorporating the kinetic model detailed in Appendix A, we obtained the microscopic rate constants that characterize the energy transfer and trapping process inside the PSU as well as the dependence of the quantum efficiency of trapping on the LH2 to LH1 protein ratio and on the wavelength of the excitation light. A high efficiency above 80% was observed in most samples/conditions. Within the near infrared absorption band of bacteria the efficiency decreases toward shorter excitation wavelengths; at fixed excitation wavelengths the efficiency declines in correlation with the LH2/LH1 ratio. Neglecting any losses due to LH2, unique values of exciton trapping time (60.7 ps) and trapping efficiency (88.1%) were obtained irrespective to the sample. Our data also detect a small number of disconnected LH2 complexes, particularly in HL adapted samples. The slower energy transfer in LL membranes is offset by having larger peripheral LH2 antenna network, which from the perspective of their ecological habitat facilitates life under low light environments. Moreover, the similarity of the calculated quantum efficiencies for all samples implies a robust mechanism for the primary processes of charge separation in photosynthesis.

Acknowledgements

This work was supported by the Estonian Research Council (grant IUT02-28) and the ESF DoRa 4 program (grant NLOFY12523T). C.N.H. was supported by funding from the Biotechnology and Biological Sciences Research Council (UK) and as part of the Photosynthetic Antenna Research Center (PARC), an Energy Frontier Research Center funded by

the US Department of Energy, Office of Science, and Office of Basic Energy Sciences under Award Number DE-SC0001035. We are grateful to J. Olsen for the expert help in the preparation of the samples and to J. Snellenburg for the insightful discussions concerning data analysis methods.

Appendix A

Fig. A1 presents a kinetic model used in this study to describe the population dynamics of excited LH2 and LH1 chlorophylls in the photosynthetic unit of purple bacteria.

The system of kinetic equations corresponding to the scheme shown in Fig. A1 without the unconnected LH2 compartment is:

$$\begin{aligned} dA/dt &= -k_1 A - k_{\text{loss}} A + k_{-1} B \\ dB/dt &= k_1 A - k_{-1} B - k_2 B \end{aligned} \tag{A1}$$

where $A(t)$ marks the population of the B850 excitons in LH2, $B(t)$ marks that of the B880 excitons in LH1, and k_2 stands either for k_2^0 or for k_2^c, depending on the state of RCs.

The solution of Fig. A1 describing the observed decay curves is given by

$$\begin{aligned} A(t) &= a_1 e^{-\gamma_1 t} + a_2 e^{-\gamma_2 t}, \\ B(t) &= b_1 e^{-\gamma_1 t} + b_2 e^{-\gamma_2 t}, \end{aligned} \tag{A2}$$

where γ_1 and γ_2 are the apparent (experimental) rate constants, and a_1, a_2, b_1, and b_2 are the time-independent coefficients that depend on k_1, k_{loss}, k_{-1}, k_2 as well as the initial populations of excitations, $A(0)$ and $B(0)$. The factors $\exp(-\gamma_1 t)$ and $\exp(-\gamma_2 t)$ are assumed to be zero for $t < 0$.

The apparent rate constants are related to the microscopic rate constants as follows [48]:

$$\begin{aligned} \gamma_1 &= \frac{1}{2}\left[(k_{\text{loss}} + k_1 + k_{-1} + k_2) + \sqrt{(k_{\text{loss}} + k_1 - k_{-1} - k_2)^2 + 4k_1 k_{-1}}\right] \\ \gamma_2 &= \frac{1}{2}\left[(k_{\text{loss}} + k_1 + k_{-1} + k_2) - \sqrt{(k_{\text{loss}} + k_1 - k_{-1} - k_2)^2 + 4k_1 k_{-1}}\right]. \end{aligned} \tag{A3}$$

It is assumed that k_2 depends on the state of RC switching between two values, whereas k_1 and k_{-1} are independent from the RC state. However, under equilibrium conditions, the forward and backward transfer rates, k_1 and k_{-1}, are supposed to be related to each other via the Boltzmann factor. The equilibrium constant defined as $K = k_1 / k_{-1}$ is given:

$$K = \frac{k_1}{k_{-1}} = \frac{\text{LH1}}{\text{LH2}} \frac{N_{\text{LH1}}}{N_{\text{LH2}}} e^{-\frac{\Delta E}{k_B T}}, \tag{A4}$$

where LH1/LH2 is the ratio of the core and peripheral antenna complexes, N_{LH1} and N_{LH2} are the numbers of the BChl chromophores in the B875 and B850 arrangements in LH1 and LH2, respectively, and ΔE is the energy gap between the lowest-energy exciton states of LH1 and LH2. From the structure of light harvesting antennas of *R. sphaeroides* with PufX protein, it is known that $N_{LH2} = 18$ and $N_{LH1} = 56$ [41]. For simplicity, ΔE is defined as the difference between the LH1 and LH2 absorption maxima, obtained by the decomposition of the absorption spectra of the membrane samples, as described in Section 3.1.

The steady state excited state populations can be deduced from the system of kinetic equations

$$\begin{aligned} (k_1 + k_{\text{loss}})A - k_{-1} B &= jP \\ -k_1 A + (k_{-1} + k_2)B &= (1-j)P, \end{aligned} \tag{A5}$$

where P is the excitation rate that is proportional to the power of incident light, and j and $(1 - j)$ describe the branching of excitation between the LH2 and LH1 compartments, respectively. By solving this system of equations the steady state fluorescence yield ratio, F850/F880, can be expressed as

$$\frac{F_{850}}{F_{880}} = \frac{A}{B} = \frac{k_{-1} + jk_2}{k_1 + k_{\text{loss}}(1-j)}. \tag{A6}$$

The quantum efficiency of the primary stage of photosynthesis, defined as the probability that an absorbed photon leads to the charge separation in a RC [25], can be calculated as the ratio of the trapping rate of the LH1 excitons by open RCs divided by P, the rate of excitation by the incoming light. Under steady state excitation the trapping rate by open RCs is given by $k_t^0 B$, where k_t^0 is the trapping rate constant in the case of open RC and B is the steady state population of LH1 excitons. By expressing B from Eq. (A5) through the rate constants the equation for the quantum efficiency takes the form:

$$\eta = \frac{k_t^0 B}{P} = k_t^0 \frac{1 + k_{\text{loss}}(1-j)/k_1}{k_2^0 + k_{\text{loss}}(1/K + k_2^0/k_1)}. \tag{A7}$$

In the case of $k_{\text{loss}} = 0$, Eq. (A7) reduces to Eq. (3), $\eta = k_t^0 / k_2^0$, that accounts for only the population losses in LH1 [50–53].

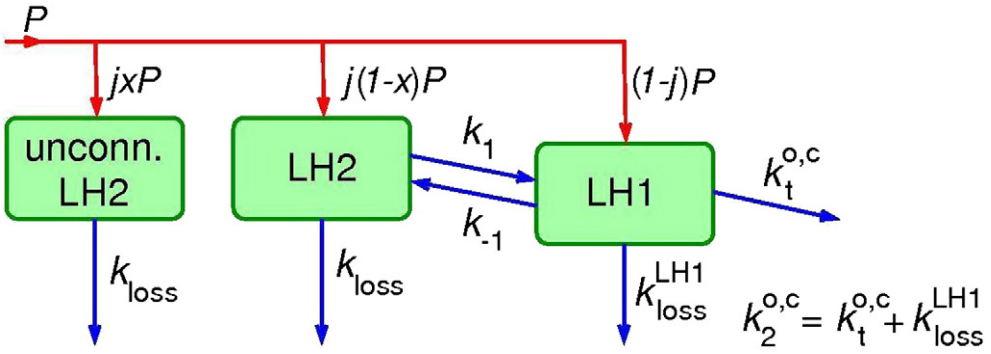

Fig. A1. Schematic illustration of the processes that determine the population dynamics of LH2, unconnected LH2, and LH1 excitons following optical excitation. Red arrows illustrate the partition of the total population rate by light absorption, P, between the unconnected LH2, LH2 and LH1 compartments. k_1 and k_{-1} are, respectively, the forward and backward energy transfer rate constants between LH2 and LH1; k_{loss} is the rate constants of any other kind of decay of LH2 excitons apart from their transfer between the complexes; $k_{\text{loss}}^{\text{LH1}}$ is a similar rate constant for LH1 excitons apart from their transfer to LH1 and RC; $k_t^{o,c}$ are the rate constants of the LH1 exciton trapping by open and closed RCs; $k_2^{o,c}$ are the (total) decay rate constants of LH1 excitons in the case of open and closed RCs.

The steady state excited state populations in the presence of unconnected peripheral antenna complexes can be deduced from the following system of kinetic equations:

$$\begin{aligned} k_{\mathrm{loss}}C &= jxP, \\ (k_1+k_{\mathrm{loss}})A - k_{-1}B &= j(1-x)P, \\ -k_1A + (k_{-1}+k_2)B &= (1-j)P, \end{aligned} \tag{A8}$$

where A and C are the populations of excited LH2 complexes that are, respectively, connected and disconnected with the core RC–LH1 complexes, B is the population of excited LH1 complexes, P is the excitation rate that is proportional to the power of incident light, and x is the relative fraction of disconnected LH2s ($0 < x < 1$). The system of Eq. (A8) can be solved for A, B and C, for instance, by the method of determinants. The steady state fluorescence yield ratio is then given by:

$$\frac{F_{850}}{F_{880}} = \frac{A+C}{B} = \frac{k_{-1}+jk_2(1+xk_1/k_{\mathrm{loss}})}{k_1(1-jx)+k_{\mathrm{loss}}(1-j)}, \tag{A9}$$

and the quantum efficiency by:

$$\eta = k_{\mathrm{t}}^0 \frac{1-jx+k_{\mathrm{loss}}(1-j)/k_1}{k_2^0+k_{\mathrm{loss}}(1/K+k_2^0/k_1)}. \tag{A10}$$

By expanding Eq. (A10) to the Taylor series by k_{loss} and keeping only the first order term the quantum efficiency can be approximated as:

$$\eta = \frac{qk_{\mathrm{t}}^0}{k_2^0}\left[1-jx-k_{\mathrm{loss}}\left(\frac{j(1-x)}{k_1}+\frac{1-jx}{k_2^0K}\right)\right], \tag{A11}$$

where the reduction in efficiency in the case of disconnected LH2 ($x > 0$) or loss from LH2 ($k_{loss} > 0$) is explicit. A calculation by the approximate Eq. (A11) using typical parameters from this study revealed less than 2% difference compared with that by exact Eq. (A10).

References

[1] A. Freiberg, Coupling of antennas to reaction centers, in: R.E. Blankenship, M.T. Madigan, C.E. Bauer (Eds.), Anoxygenic Photosynthetic Bacteria, Kluwer Academic Publishers, Dordrecht, The Netherlands, 1995, pp. 385–398.

[2] H. Gaffron, K. Wohl, Zur Theorie der Assimilation, Naturwissenschaften 24 (1936) 103–107.

[3] X. Hu, T. Ritz, A. Damjanovic, F. Autenrieth, K. Schulten, Photosynthetic apparatus of purple bacteria, Q. Rev. Biophys. 35 (2002) 1–62.

[4] W.J. Vredenberg, L.M.N. Duysens, Transfer of energy from bacteriochlorophyll to a reaction centre during bacterial photosynthesis, Nature 4865 (1963) 355–357.

[5] R.J. Cogdell, A. Gall, J. Köhler, The architecture and function of the light-harvesting apparatus of purple bacteria: from single molecules to in vivo membranes, Q. Rev. Biophys. 39 (2006) 227–324.

[6] H. Van Amerongen, L. Valkunas, R. Van Grondelle, Photosynth. Excitons (2000) 590.

[7] G. Drews, Structure and functional organization of light-harvesting complexes and photochemical reaction centers in membranes of phototrophic bacteria, Microbiol. Rev. 49 (1985) 59–70.

[8] G.D. Scholes, T. Mirkovic, D.B. Turner, F. Fassioli, A. Buchleitner, Solar light harvesting by energy transfer: from ecology to coherence, Energy Environ. Sci. 5 (2012) 9374–9393.

[9] G.D. Scholes, G.R. Fleming, A. Olaya-Castro, R. van Grondelle, Lessons from nature about solar light harvesting, Nat. Chem. 3 (2011) 763–774.

[10] A. Freiberg, M. Pajusalu, M. Rätsep, Excitons in intact cells of photosynthetic bacteria, J. Phys. Chem. B 117 (2013) 11007–11014.

[11] S. Scheuring, J.N. Sturgis, Chromatic adaptation of photosynthetic membranes, Science 309 (2005) 484–487.

[12] P.G. Adams, C.N. Hunter, Adaptation of intracytoplasmic membranes to altered light intensity in *Rhodobacter sphaeroides*, Biochim. Biophys. Acta Bioenerg. 1817 (2012) 1616–1627.

[13] S. Scheuring, R. Nevo, L.-N. Liu, S. Mangenot, D. Charuvi, T. Boudier, V. Prima, P. Hubert, J.N. Sturgis, Z. Reich, The architecture of *Rhodobacter sphaeroides* chromatophores, Biochim. Biophys. Acta Bioenerg. 1837 (2014) 1263–1270.

[14] M.B. Evans, A.M. Hawthornthwaite, R.J. Cogdell, Isolation and characterization of the different B800-850 light-harvesting complexes from low- and high-light grown cells of Rhodopseudomonas palustris, strain 2.1.6, Biochim. Biophys. Acta 1016 (1990) 71–76.

[15] N. Hartigan, H.A. Tharia, F. Sweeney, A.M. Lawless, M.Z. Papiz, The 7.5-Å electron density and spectroscopic properties of a novel low-light B800 LH2 from *Rhodopseudomonas palustris*, Biophys. J. 82 (2002) 963–977.

[16] K. McLuskey, S.M. Prince, R.J. Cogdell, N.W. Isaacs, The crystallographic structure of the B800–820 LH3 light-harvesting complex from the purple bacteria *Rhodopseudomonas acidophila* strain 7050, Biochemistry 40 (2001) 8783–8789.

[17] A. Freiberg, K. Timpmann, G. Trinkunas, Spectral fine-tuning in excitonically coupled cyclic photosynthetic antennas, Chem. Phys. Lett. 500 (2010) 111–115.

[18] V.I. Godik, A.Y. Borisov, Excitation trapping by different states of photosynthetic reaction centers, FEBS Lett. 82 (1977) 355–358.

[19] A.Y. Borisov, V.I. Godik, E.A. Kotova, V.D. Samuilov, Membrane potential effect on nanosecond recombination luminescence in *Rhodospirillum rubrum*, FEBS Lett. 119 (1980) 121–124.

[20] A.Y. Borisov, A.M. Freiberg, V.I. Godik, K. Rebane, K. Timpmann, Kinetics of picosecond bacteriochlorophyll luminescence in vivo as a function of the reaction center state, Biochim. Biophys. Acta 807 (1985) 221–229.

[21] M. Vos, R.J. Van Dorssen, J. Amesz, R. Van Grondelle, C.N. Hunter, The organization of the photosynthetic apparatus of *Rhodobacter sphaeroides*: studies of antenna mutants using singlet-singlet quenching, Biochim. Biophys. Acta 933 (1988) 132–140.

[22] A. Freiberg, V.I. Godik, K. Timpmann, Excitation energy transfer in bacterial photosynthesis studied by picosecond laser spectrochronography, in: C. Sybesma (Ed.), Advances in Photosynthesis Research, Nijhoff, Hague, The Netherlands, 1984, pp. 45–48.

[23] L. Valkunas, V. Liuolia, A. Freiberg, Picosecond processes in chromatophores at various excitation intensities, Photosynth. Res. 27 (1991) 83–95.

[24] A. Freiberg, V.I. Godik, T. Pullerits, K. Timpman, Picosecond dynamics of directed excitation transfer in spectrally heterogeneous light-harvesting antenna of purple bacteria, Biochim. Biophys. Acta 973 (1989) 93–104.

[25] F. Fassioli, A. Olaya-Castro, S. Scheuring, J.N. Sturgis, N.F. Johnson, Energy transfer in light-adapted photosynthetic membranes: from active to saturated photosynthesis, Biophys. J. 97 (2009) 2464–2473.

[26] L. Lüer, V. Moulisová, S. Henry, D. Polli, T.H.P. Brotosudarmo, S. Hoseinkhani, D. Brida, G. Lanzani, G. Cerullo, R.J. Cogdell, Tracking energy transfer between light harvesting complex 2 and 1 in photosynthetic membranes grown under high and low illumination, Proc. Natl. Acad. Sci. 109 (2012) 1473–1478.

[27] P.J. Kiley, S. Kaplan, Molecular genetics of photosynthetic membrane biosynthesis in *Rhodobacter sphaeroides*, Microbiol. Rev. 52 (1988) 50–69.

[28] J. Zeilstra-Ryalls, M. Gomelsky, J.M. Eraso, A. Yeliseev, J. O'Gara, S. Kaplan, Control of photosystem formation in *Rhodobacter sphaeroides*, J. Bacteriol. 180 (1998) 2801–2809.

[29] C.A. Siebert, P. Qian, D. Fotiadis, A. Engel, C.N. Hunter, P.A. Bullough, Molecular architecture of photosynthetic membranes in *Rhodobacter sphaeroides*: the role of PufX, EMBO J. 23 (2004) 690–700.

[30] P. Qian, P.A. Bullough, C.N. Hunter, Three-dimensional reconstruction of a membrane-bending complex: the RC–LH1–P*u*fx core dimer of *Rhodobacter sphaeroides*, J. Biol. Chem. 283 (2008) 14002–14011.

[31] P. Qian, M.Z. Papiz, P.J. Jackson, A.A. Brindley, I.W. Ng, J.D. Olsen, M.J. Dickman, P.A. Bullough, C.N. Hunter, Three-dimensional structure of the *Rhodobacter sphaeroides* RC–LH1–PufX complex: dimerization and quinone channels promoted by PufX, Biochemistry 52 (2013) 7575–7585.

[32] W.P. Barz, A. Vermeglio, F. Francia, G. Venturoli, B.A. Melandri, D. Oesterhelt, Role of the PufX protein in photosynthetic growth of *Rhodobacter sphaeroides*. 2. PufX is required for efficient ubiquinone/ubiquinol exchange between the reaction center QB site and the cytochrome bc1 complex, Biochemistry 34 (1995) 15248–15258.

[33] R.J. Cogdell, P.K. Fyfe, S.J. Barrett, S.M. Prince, A.A. Freer, N.W. Isaacs, P. McGlynn, C.N. Hunter, The purple bacterial photosynthetic unit, Photosynth. Res. 48 (1996) 55–63.

[34] M.L. Cartron, J.D. Olsen, M. Sener, P.J. Jackson, A.A. Brindley, P. Qian, M.J. Dickman, G. J. Leggett, K. Schulten, C. Neil Hunter, Integration of energy and electron transfer processes in the photosynthetic membrane of *Rhodobacter sphaeroides*, Biochim. Biophys. Acta Bioenerg. (2014) (in press).

[35] M.R. Jones, G.J.S. Fowler, L.C.D. Gibson, G.G. Grief, J.D. Olsen, W. Crielaard, C.N. Hunter, Mutants of *Rhodobacter sphaeroides* lacking one or more pigment–protein complexes and complementation with reaction-center, LH1, and LH2 genes, Mol. Microbiol. 6 (1992) 1173–1184.

[36] J.D. Olsen, G.D. Sockalingum, B. Robert, C.N. Hunter, Modification of a hydrogen bond to a bacteriochlorophyll a molecule in the light-harvesting 1 antenna of *Rhodobacter sphaeroides*, Proc. Natl. Acad. Sci. U. S. A. 91 (1994) 7124–7128.

[37] R.K. Clayton, S.C. Straley, Photochemical electron transport in photosynthetic reaction centers. IV. Observations related to the reduced photoproducts, Biophys. J. 12 (1972) 1221–1234.

[38] A. Freiberg, P. Saari, Picosecond spectrochronography, IEEE J. Quantum Electron. QE-19 (1983) 622–630.

[39] A. Freiberg, Primary processes of photosynthesis studied by fluorescence spectroscopy methods, Laser Chem. 6 (1986) 233–252.

[40] A. Freer, S. Prince, K. Sauer, M. Papiz, A. Hawthornthwaite-Lawless, G. McDermott, R. Cogdell, N.W. Isaacs, Pigment–pigment interactions and energy transfer in the antenna complex of the photosynthetic bacterium *Rhodopseudomonas acidophila*, Structure 4 (1996) 449–462.

[41] M. Şener, J. Strümpfer, J.A. Timney, A. Freiberg, C.N. Hunter, K. Schulten, Photosynthetic vesicle architecture and constraints on efficient energy harvesting, Biophys. J. 99 (2010) 67–75.

[42] R. Van Grondelle, Excitation energy transfer, trapping and annihilation in photosynthetic systems, Biochim. Biophys. Acta 811 (1985) 147–195.

[43] J.G.C. Bakker, R. Van Grondelle, W.T.F. Den Hollander, Trapping, loss and annihilation of excitations in a photosynthetic system. II. Experiments with the purple bacteria *Rhodospirillum rubrum* and *Rhodopseudomonas capsulata*, Biochim. Biophys. Acta 725 (1983) 508–518.

[44] G. Paillotin, N.E. Geacintov, J. Breton, A master equation theory of fluorescence induction, photochemical yield, and singlet-triplet exciton quenching in photosynthetic systems, Biophys. J. 44 (1983) 65–77.
[45] P.G. Adams, D.J. Mothersole, I.W. Ng, J.D. Olsen, C.N. Hunter, Monomeric RC–LH1 core complexes retard LH2 assembly and intracytoplasmic membrane formation in PufX-minus mutants of *Rhodobacter sphaeroides*, Biochim. Biophys. Acta Bioenerg. 1807 (2011) 1044–1055.
[46] J.D. Olsen, J.D. Tucker, J.A. Timney, P. Qian, C. Vassilev, C.N. Hunter, The organization of LH2 complexes in membranes from *Rhodobacter sphaeroides*, J. Biol. Chem. 283 (2008) 30772–30779.
[47] K. Leiger, L. Reisberg, A. Freiberg, Fluorescence micro-spectroscopy study of individual photosynthetic membrane vesicles and light-harvesting complexes, J. Phys. Chem. B 117 (2013) 9315–9326.
[48] H.W. Trissl, C.J. Law, R.J. Cogdell, Uphill energy transfer in LH2-containing purple bacteria at room temperature, Biochim. Biophys. Acta 1412 (1999) 149–172.
[49] K.L. Zankel, R.K. Clayton, Uphill energy transfer in a photosynthetic bacterium, Photochem. Photobiol. 9 (1969) 7–15.
[50] A. Freiberg, J.P. Allen, J. Williams, N.W. Woodbury, Energy trapping and detrapping by wild type and mutant reaction centers of purple non-sulfur bacteria, Photosynth. Res. 48 (1996) 309–319.
[51] K. Timpmann, F.G. Zhang, A. Freiberg, V. Sundström, Detrapping of excitation energy from the reaction center in the photosynthetic purple bacterium *Rhodospirillum rubrum*, Biochim. Biophys. Acta 1183 (1993) 185–193.
[52] K. Timpmann, A. Freiberg, V. Sundström, Energy trapping and detrapping in the photosynthetic bacterium *Rhodopseudomonas viridis*: transfer-to-trap-limited dynamics, Chem. Phys. 194 (1995) 275–283.
[53] O.J.G. Somsen, L. Valkunas, R. van Grondelle, A perturbed two-level model for exciton trapping in small photosynthetic systems, Biophys. J. 70 (1996) 669–683.
[54] X.J. Jordanides, G.D. Scholes, W.A. Shapley, J.R. Reimers, G.R. Fleming, Electronic couplings and energy transfer dynamics in the oxidized primary electron donor of the bacterial reaction center, J. Phys. Chem. B 108 (2004) 1753–1765.
[55] X.J. Jordanides, G.D. Scholes, G.R. Fleming, The mechanism of energy transfer in the bacterial photosynthetic reaction center, J. Phys. Chem. B 105 (2001) 1652–1669.
[56] A. Freiberg, V.I. Godik, T. Pullerits, K.E. Timpmann, Directed picosecond excitation transport in purple photosynthetic bacteria, Chem. Phys. 128 (1988) 227–235.
[57] K. Timpmann, A. Freiberg, V.I. Godik, Picosecond kinetics of light excitations in photosynthetic purple bacteria in the temperature range of 300–4 K, Chem. Phys. Lett. 182 (1991) 617–622.
[58] Z. Fetisova, A. Freiberg, V. Novoderezhkin, A. Taisova, K. Timpmann, Antenna size dependent exciton dynamics in the chlorosomal antenna of the green bacterium *Chloroflexus aurantiacus*, FEBS Lett. 383 (1996) 233–236.
[59] A. Freiberg, K. Timpmann, A.A. Moskalenko, N.Y. Kuznetsova, Pico- and nanosecond fluorescence kinetics of photosystem II reaction center and its complex with CP47 antenna, Biochim. Biophys. Acta 1184 (1994) 45–53.
[60] S. Caffarri, K. Broess, R. Croce, H. van Amerongen, Excitation energy transfer and trapping in higher plant photosystem II complexes with different antenna sizes, Biophys. J. 100 (2011) 2094–2103.
[61] T.G. Owens, S.P. Webb, L. Mets, R.S. Alberte, G.R. Fleming, Antenna size dependence of fluorescence decay in the core antenna of photosystem I: estimates of charge separation and energy transfer rates, Proc. Natl. Acad. Sci. 84 (1987) 1532–1536.
[62] R.G. Walters, Towards an understanding of photosynthetic acclimation, J. Exp. Bot. 56 (2005) 435–447.
[63] Govindjee, A role for a light-harvesting antenna complex of photosystem II in photoprotection, Plant Cell 14 (2002) 1663–1668 (Online).
[64] A. Freiberg, K. Timpmann, Picosecond fluorescence spectroscopy of light-harvesting antenna complexes from *Rhodospirillum rubrum* in the 300–4 K temperature range. Comparison with the data on chromatophores, J. Photochem. Photobiol. B 15 (1992) 151–158.
[65] R.A. Niederman, D.E. Mallon, L.C. Parks, Membranes of *Rhodopseudomonas sphaeroides*. VI. Isolation of a fraction enriched in newly synthesized bacteriochlorophyll a-protein complexes, Biochim. Biophys. Acta 555 (1979) 210–220.
[66] J.D. Tucker, C.A. Siebert, M. Escalante, P.G. Adams, J.D. Olsen, C. Otto, D.L. Stokes, C.N. Hunter, Membrane invagination in *Rhodobacter sphaeroides* is initiated at curved regions of the cytoplasmic membrane, then forms both budded and fully detached spherical vesicles, Mol. Microbiol. 76 (2010) 833–847.
[67] C.N. Hunter, R. Van Grondelle, N.G. Holmes, O.T.G. Jones, R.A. Niederman, Fluorescence yield properties of a fraction enriched in newly synthesized bacteriochlorophyll a-protein complexes from Rhodopseudomonas sphaeroides, Photochem. Photobiol. 30 (1979) 313–316.
[68] M. de Rivoyre, N. Ginet, P. Bouyer, J. Lavergne, Excitation transfer connectivity in different purple bacteria: a theoretical and experimental study, Biochim. Biophys. Acta Bioenerg. 1797 (2010) 1780–1794.